BBA - Gene Regulatory Mechanisms 1869 (2026) 195151

Contents lists available at ScienceDirect

BBA - Gene Regulatory Mechanisms

journal homepage: www.elsevier.com/locate/bbagrm

Nuclear export block of tyrosine-phosphorylated STAT1 facilitates rapid responsiveness to interferon-γ stimuli at the expense of signal strength

Thomas Meyer [a,*], Florian Lamprecht [b,d], Andreas Begitt [c], Thomas Höfer [b,d], Uwe Vinkemeier [c]

[a] Department of Psychosomatic Medicine and Psychotherapy, University Medical Centre Göttingen, University of Göttingen, 37073, Göttingen, Germany
[b] Division of Theoretical Systems Biology, German Cancer Research Center, Heidelberg, Germany
[c] School of Life Sciences, University of Nottingham, Nottingham, NG7 2UH, United Kingdom
[d] Bioquant Center, University of Heidelberg, Heidelberg, Germany

ARTICLE INFO

Keywords:
STAT proteins
Modeling
Nucleocytoplasmic shuttling
Tyrosine phosphorylation

ABSTRACT

Interferon-induced STAT1 (signal transducer and activator of transcription 1) signal transduction constitutes a dynamic network of concurrent activation and inactivation steps that directly transmits extracellular information from the plasma membrane to the nucleus. To elucidate how nuclear retention of tyrosine-phosphorylated STAT1 as a fundamental principle of the STAT1 network directs signal transduction, we have developed a mathematical rate equation model for STAT1 nucleocytoplasmic shuttling. Based on an interplay between experimental data on the behavior of transport variants with altered nucleocytoplasmic translocation and computational simulations, we calculated the mean residence time of phosphorylated STAT1 in the nucleus to be 13.1 min (5%–95%-CI = 1.6–48.4 min), indicating the highly dynamic nature of the STAT1 signal network. However, when we assessed the time course of unphosphorylated STAT1 from nuclear entry to its subsequent cytoplasmic exit, we found that the half-life of nuclear STAT1 in resting cells was even shorter (5.0 min, 5%–95%-CI = 0.3–15.0 min). Our data reveal that the STAT1 pathway has not evolved to achieve maximal signal amplification, but rather allows for a compromise between rapid termination and efficient signal output. Decoupling of nuclear export from its prior dephosphorylation, such that also phospho-STAT1 can unphysiologically exit the nucleus, results in an overall lower nuclear concentration of activated STAT1 throughout the entire stimulation period, demonstrating the physiological significance of the nuclear export block of phosphorylated STAT1 for cytokine-driven signal propagation. Thus, the complex dynamics of the unique STAT1 network accounts for both efficient and flexible signal transduction, particularly in the course of transient stimulation.

1. Introduction

Members of the signal transducer and activator of transcription (STAT) family directly transmit information received from extracellular cytokine stimulation to target gene expression in the nucleus [1,2]. Ligand binding to the extracellular domain of cytokine receptors induces dimerization of the receptor followed by auto-phosphorylation of Jaks (Janus kinases) that are non-covalently attached to the intracellular receptor chains [2,3]. The activated Jaks then trans-phosphorylate tyrosine residues within the cytoplasmic domain of the cytokine receptor, thereby creating docking sites for the SH2 domain of STAT proteins [1–3]. Once STAT proteins are recruited to the phosphotyrosine residues of intracellular receptor chains, Jaks catalyse the phosphorylation of a single tyrosine residue within the carboxy-terminal domain of STATs [1–3]. The STATs are then released from the receptor complex and enter the nucleus as homodimers or heterodimers where they bind to cognate regulatory DNA sequences termed GAS (γ-activated sites) and non-specifically to DNA [1].

Initially believed to be cytoplasmic proteins that enter the nucleus only after activation, it is now clear that the STATs are nucleocytoplasmic shuttling proteins both before and during the stimulation of cells with cytokines [4–6]. Best characterized in this respect is STAT1, the central mediator of the interferon response [7] (Fig. 1A, B), but there appear to be many similarities in the STAT family of proteins. Upon cytokine stimulation, tyrosine-phosphorylated STAT1 dimers are imported into the nucleus in association with importin-α5 and importin-β [8–11]. Tyrosine phosphorylation of STAT1 is reversed by phosphatases in the nucleus and the cytoplasm [12–15]. Export from the nucleus requires prior enzymatic dephosphorylation, since phospho-STAT1 is

* Corresponding author at: Department of Psychosomatic Medicine and Psychotherapy, University of Göttingen, Waldweg 33, 37073, Göttingen, Germany.
E-mail address: thomas.meyer@med.uni-goettingen.de (T. Meyer).

https://doi.org/10.1016/j.bbagrm.2026.195151
Received 4 December 2025; Received in revised form 24 February 2026; Accepted 17 March 2026
Available online 24 March 2026

Abbreviations

GAS	γ-activated site
GFP	green fluorescent protein
IFN-γ	interferon-γ
NES	nuclear export signal
NLS	nuclear localization signal
STAT	signal transducer and activator of transcription

precluded from nuclear exit [16]. In contrast, unphosphorylated STAT1 is capable both of carrier-independent translocation via direct interactions with the proteins of the nuclear pore and carrier-dependent nuclear export mediated by the exportin Crm1 [16–18].

Both the latent, unphosphorylated STAT1 and the active, phosphorylated STAT1 exist as monomers and homodimers [19]. Latent STAT1 dimerizes through reciprocal interactions between the coiled-coil domain of one protomer and the DNA-binding domain of the partner protomer, leading to an antiparallel dimer conformation [20–22]. Additionally, reciprocal N-terminal interactions have been described which are required for cooperative DNA-binding and subsequent transcriptional activation [21–24]. In contrast, active STAT1 forms phosphotyrosine/SH2 domain dimers oriented in a parallel conformation [25]. The two kinds of STAT1 dimers in antiparallel and parallel conformation are formed with approximately the same affinity [26]. In addition, the signal that emanates from the cytokine receptor is modulated by numerous interactions of cytokine receptors, Jaks and STATs with regulatory proteins that influence the activation-inactivation cycle, DNA binding, and/or protein solubility by SUMO (small ubiquitin-like modifier) [1–3,27–31]. However, the regulatory potential that is inherent in the dynamic redistribution of the shuttling STAT1 signal transducer has gained relatively little attention.

In the present work, we have used a combination of quantitative measurements of STAT1 activation, targeted mutagenesis, and mathematical modeling to examine the Jak-STAT1 network (Supplementary Data 1). Focusing on the critical role of the well-established nuclear export block of tyrosine-phosphorylated STAT1, we have analyzed the circular signaling network by experimentally altering nuclear transport properties of the STAT1 molecule. Due to its complexity, we have addressed only the STAT1 core network, while post-translational modifications of STAT1 transcription factors, such as sumoylation, serine and threonine phosphorylation, as well as oligomerization due to cooperative DNA binding were not considered, all of which are known to influence signal strength. In particular, we examined the functional significance of nuclear retention of tyrosine-phosphorylated STAT1 for the propagation of cytokine-induced signals. Here we demonstrate how a disrupted network design with altered transport processes influences the outcome of cytokine signaling both in terms of signal strength and duration. Using this multi-dimensional approach including the transient expression of translocation variants with abnormal nucleocytoplasmic shuttling behaviors in two different human cell lines (HeLa and U3A cells), we found that the STAT1 pathway operates remote from maximal signal propagation. Nevertheless, the most striking finding is that the complex dynamics of the STAT1 network account for both efficient and flexible signal transduction particularly at low activation levels.

2. Materials and methods

2.1. Cell culture

HeLa cells expressing endogenous STAT1 and U3A fibrosarcoma cells lacking endogenous STAT1 expression were cultured at 37 °C in a humidified 5% CO_2 atmosphere in Dulbecco's modified Eagle's medium supplemented with 10% FCS (fetal calf serum; Gibco), 1% penicillin/streptavidin and 1% amphotericin. Cells were transiently transfected with STAT1-coding plasmids using the Lipofectamine plus (Gibco) method and 24 h after transfection stimulated with 5 ng/ml IFN-γ (human interferon-γ; Biomol). In some experiments, cells were additionally incubated with 500 nM staurosporine (Merck), 10 ng/ml leptomycin B (LMB; Merck), or a combination of 0.8 mM sodium vanadate and 0.2 mM H_2O_2. For immunofluorescence experiments, cells were grown on poly-L-lysine-coated glass coverslips and 24 h after transient transfection were stimulated with 5 ng/ml IFN-γ.

2.2. Plasmid construction

The cDNA expressing full-length human STAT1 (amino acids 1–746) was cloned into pEGFP-N1 to generate STAT1-WT fused C-terminally to green fluorescent protein [32]. A STAT1 import variant lacking a functional NLS (nuclear localization signal) due to substitutions of the two lysines in position 410 and 413 to glutamic acids was termed here ΔNLS [4]. In addition, a STAT1-NES variant with a heterotopic NES (nuclear export signal) was cloned by ligating a PCR fragment amplified from pGST-STAT1$^{367–427}$-GFP [4] into the *BamHI-NotI* restriction sites of pSTAT1-GFP. The resulting plasmid pSTAT1-NES-GFP coded for a transferable NES activity containing amino acids 367–427 of STAT1 situated between the cDNAs for wild-type (WT) STAT1 and GFP [24]. Plasmids coding for STAT1 import variants were generated by phosphorylating annealed oligonucleotides in a T4 polynucleotide kinase reaction and subsequently cloning them into the *Bam*HI site of pSTAT1-GFP, which is situated between the cDNAs for STAT1 and GFP. The following oligonucleotide pairs were used:

(i) wNLS: 5′-GATCCCAAAAAAAAGGCGAAGGTCGAGGCG-′3 and 5′-GATCCGCCTCGACCTTCGCCTTTTTTTTGG-′3;
(ii) sNLS: 5′-GATCCCAAAAAAAAGCGCAAGGTCGAGGCG-′3 and 5′-GATCCGCCTCGACCTTGCGCTTTTTTTTGG-′3;
(iii) LSN: 5′-GATCCCAAAGAGGCGAAAGTCAAAAAGGCG-′3 and 5′-GATCCGCCTTTTTGACTTTCGCCTCTTTGG-′3.

pSTAT1-wNLS coded for a mutated NLS derived from the large T antigen of SV40 virus (PKKKAKVE; mutation underlined) and pSTAT1-sNLS for a tandem arrangement of the native SV40 NLS (PKKKRKVE), while in pSTAT1-LSN this sequence was permutated (PKEAKVKK). Fig. 1C summarizes the different constructs used in this study.

2.3. Fluorescence microscopy

For direct microscopical examination, the cells were fixed in 3.7% paraformaldehyde in PBS (phosphate-buffered saline), and subsequently, the nuclei were stained with 5 mg/ml Hoechst 33258 (Merck). The kinetics of IFN-γ-induced nuclear accumulation of STAT1-GFP-NES were monitored in transfected U3A cells by a combination of direct and indirect fluorescence microscopy. Briefly, cells grown on 8-well chamber slides were transiently transfected with pSTAT1-GFP-NES and on the next day treated with IFN-γ for the indicated times. Cells were fixed with methanol for 15 min at −20 °C before they were permeabilized with 1% Triton X-100 in PBS for 20 min at room temperature. The cells were treated for 45 min with 25% FCS in PBS to saturate non-specific binding sites and subsequently incubated for an additional 45 min with the phospho-tyrosine-specific STAT1 antibody diluted 1:1000 in 25% FCS in PBS. After three washes with PBS, a Cy3-coupled secondary antibody was added for 45 min and finally the nuclei were stained for an additional 10 min with 5 μg/ml of Hoechst dye 33258. Samples were mounted in fluorescence mounting medium (Southern Biotech) and the intracellular fluorescence localization visualized using a Zeiss Axioplan microscope (Zeiss) equipped with the appropriate fluorescence filters.

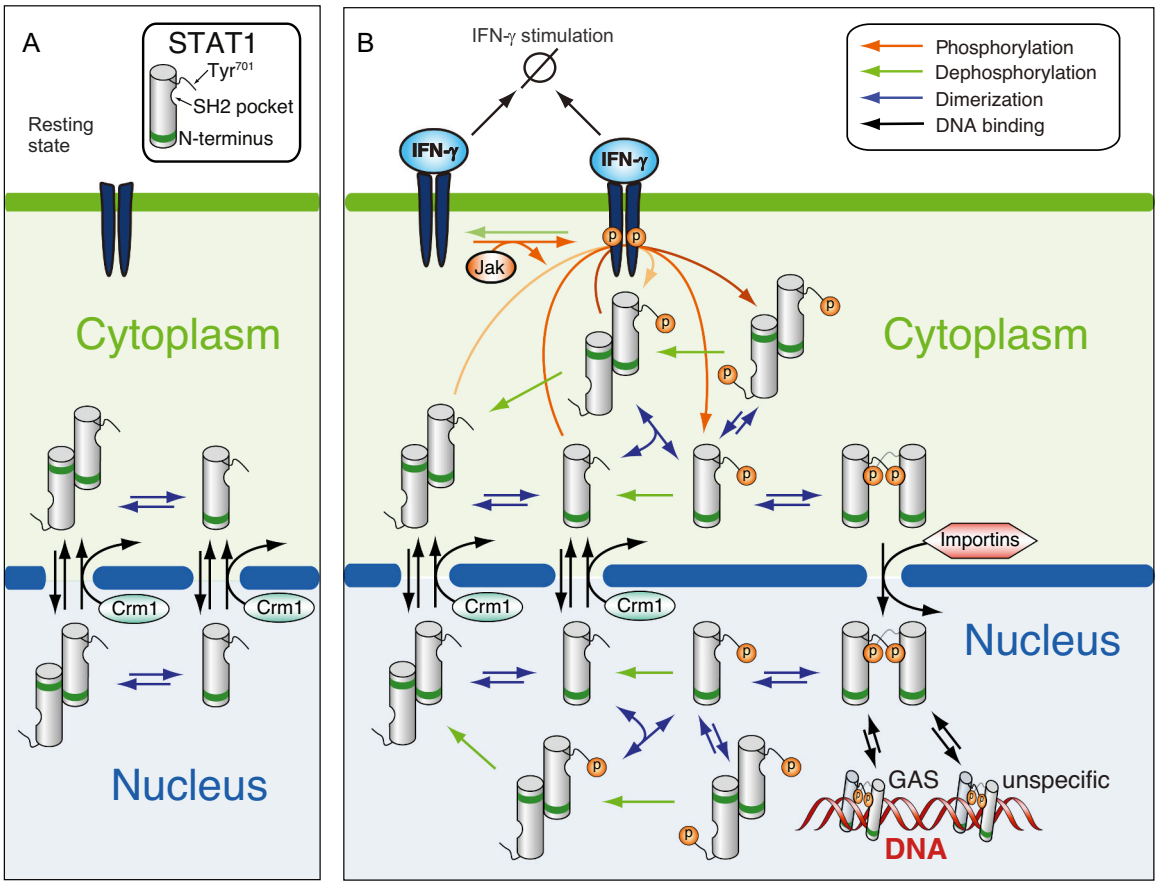

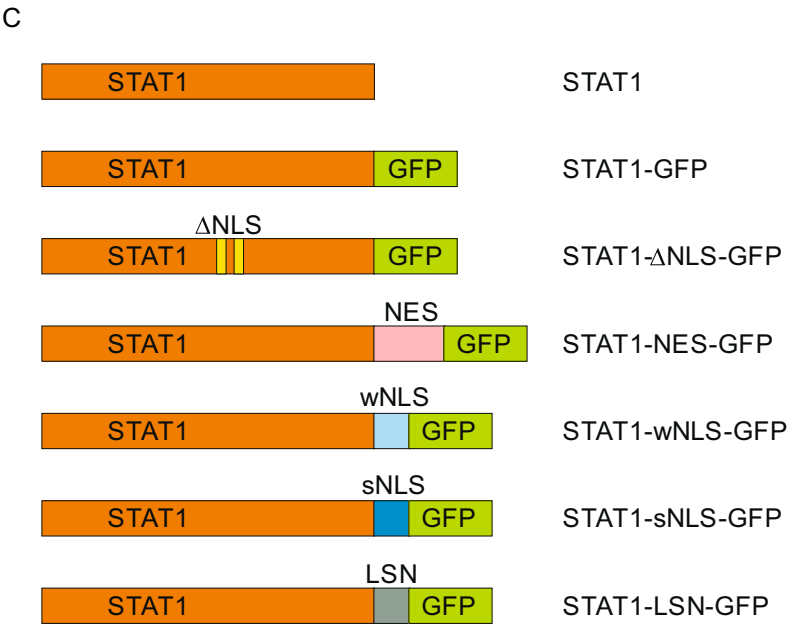

Fig. 1. Pathway design of the STAT1 nucleocytoplasmic circuits in the absence (A) and presence (B) of a cytokine stimulus. (A) Network model for STAT1 translocation in resting cells with nuclear import and export of latent STAT1 as monomers and antiparallel dimers. CRM1 denotes energy-dependent nuclear export via the export receptor CRM1. (B) Network model for IFN-γ-stimulated STAT1 signal transduction depicting nuclear import and export of latent STAT1, activation of IFN-γ receptor/Jak complexes, STAT1 binding to activated IFN-γ receptor/Jak complexes, tyrosine phosphorylation and dimerization of STAT1, nuclear import of phospho-STAT1, specific (GAS) and non-specific binding of phospho-STAT1 to DNA, and cytoplasmic and nuclear dephosphorylation. (C) Schematic presentation of STAT1 expression constructs used in this study; GFP; green fluorescent protein, LSN; scrambled nuclear localization signal, NES; nuclear export signal, ΔNLS; K410E,K413E, sNLS; strong nuclear localization signal, wNLS; weak nuclear localization signal.

2.4. Protein extraction

One day after transfection, HeLa or U3A cells expressing recombinant STAT1 variants grown on 6-well plates were stimulated with IFN-γ for the indicated times and concentrations. Cells were then lysed on ice for 5 min in 60 µl of cytoplasmic extraction buffer (20 mM HEPES, pH 7.4, 10 mM KCl, 10% (*v*/v) glycerol, 1 mM EDTA, 0.1 mM Na_3VO_4, 0.1% IGEPAL-CA-360, 3 mM 1,4-dithiothreitol (DTT), 0.4 mM Pefabloc (Sigma-Aldrich), and Complete Mini protease inhibitors (Roche)). The lysates were centrifuged at 4 °C and 16,000*g* for 30 s. The resulting supernatants from this step were centrifuged again at 16,000*g* for 5 min and collected as cytoplasmic extracts. Nuclear extracts were prepared by adding 60 µl of nuclear extraction buffer (20 mM HEPES, pH 7.4, 420 mM KCl, 20% (*v*/v) glycerol, 1 mM EDTA, 0.1 mM Na_3VO_4, 3 mM DTT, 0.4 mM Pefabloc, and Complete Mini protease inhibitors) to the pellets from the first centrifugation step. Extraction was performed on ice for 30 min prior to centrifugation at 4 °C and 16,000*g* for 15 min. Equal volumes of nuclear extracts were mixed with cytoplasmic extracts from the same cells to generate whole cell lysates.

2.5. Western blotting

Protein lysates prepared in 6× SDS sample buffer were subjected to SDS polyacrylamide gel electrophoresis, followed by immunoblotting. The separation gel was prepared from 10% Rotiphorese Gel 30 (acrylamide/bisacrylamide; ratio 37.5:1), 0.03% ammonium persulfate (APS), and 0.16% *N*,*N*,*N*′,*N*′-tetramethylethylenediamine (TEMED) in 4× separation gel buffer containing 1.5 M Tris-HCl and 0.4% SDS, pH 8.8. The stacking gel consisted of a 5% acrylamide/bisacrylamide (37.5:1) solution, 0.06% APS, and 0.2% TEMED in stacking gel buffer (0.5 M Tris-HCl, 0.4% SDS, pH 6.8). Protein samples were loaded onto the gel and separated electrophoretically at a constant current of 11 mA. Subsequently, proteins were transferred to polyvinylidene difluoride membranes for 90 min at 80 mA per gel using a semi-dry blotting system. Following transfer, membranes were blocked for 60 min at room temperature in 4% BSA (bovine serum albumin) prepared in TBS-T (137 mM NaCl, 10 mM Tris-HCl, pH 7.4, 0.1% Tween-20) with gentle agitation. Blocked membranes were incubated overnight at 4 °C with primary antibodies diluted in blocking buffer. Phospho-STAT1 was detected in cell lysates by means of immunoblotting using a polyclonal antibody specific for phospho-STAT1-Tyr701 (New England Biolabs) followed by incubation with a horseradish peroxidase-conjugated secondary antibody. After stripping off bound immunoglobulins, the membranes were re-exposed to the polyclonal STAT1-specific antibody C-24 (Santa Cruz). The intensities of the band signals were densitometrically determined using the enhanced chemiluminescence reaction, and the experiment was repeated in three biological replicates. The purity of the extract was tested using antibodies against the nuclear transcription factor Sp1 and the cytoplasmic Eps15 (both from Santa Cruz; Supplementary Data 2).

2.6. Electrophoretic mobility shift assay

To rule out that the NLS variants may have abnormal DNA binding resulting in their predominant nuclear localization, competition gelshift experiments were performed. Briefly, whole cell extracts from IFN-γ-stimulated, STAT1-reconstituted U3A cells expressing GFP-tagged fusions of either WT or mutant protein were prepared and the lysates subsequently incubated with 1 ng of a [^{33}P]-labeled duplex oligonucleotide probe containing a high-affinity binding site (M67). Radioactive labeling of the M67 GAS element (sequence: 5′-CGA-CATTTCCCGTAAATCTG-′3 without Poly-T overhang) was achieved by an end-filling reaction using the Klenow fragment (New England Biolabs). Four microliters of the cellular extract were mixed with [^{33}P]-labeled duplex oligonucleotide in EMSA buffer and left for 15 min at room temperature. Subsequently, a 750-fold molar excess of unlabeled M67 DNA was added on ice for an additional 0, 15 or 30 min, before the reactions were loaded on the running 4% 29:1 acrylamide:bisacrylamide gel and separated at 400 V. The DNA dissociation kinetics were visualized autoradiographically on vacuum-dried gels with a phosphoimaging system (FLA-5100, Fuji) using the programs Aida Image Analyzer v. 4.06 and TINA 2.0 (Raytest).

2.7. Reporter gene assay

Gene expression by the NLS variants was examined in transiently transfected U3A cells and compared to the WT protein. Cells grown in 48-well plates were co-transfected with the respective STAT1 expression plasmid (250 ng), a constitutively expressed β-galactosidase plasmid (200 ng), and a luciferase-encoding plasmid (70 ng). The reporter construct contained three copies of an IFN-γ-inducible *Ly6E* GAS element from the promoter region of the lymphocyte antigen 6 complex locus E upstream of the transcription start site. On the next day, the transfected cells were either left untreated or stimulated for 6 h with IFN-γ, before cellular proteins were lysed in a buffer containing 25 mM glycylglycine, 1% Triton X-100, 15 mM $MgSO_4$, 4 mM EGTA, 0.4 mM Pefabloc, 3 mM DTT, pH 7.8, and Complete protease inhibitors. Luciferase expression was measured using the luciferase assay substrate solution from Promega in the Tecan Spark multimode microplate reader (Tecan Group). Luciferase activity was normalized to the corresponding β-galactosidase activity, which was measured spectroscopically at 420 nm. For every construct and stimulation mode, six independent transfections were tested, and the experiment was repeated in triplicate.

2.8. Reverse transcriptase-PCR

The transcriptional activities were assessed by means of reverse transcriptase-PCR. Similar cell numbers of transfected U3A cells expressing either WT or mutant STAT1 were stimulated with IFN-γ for the indicated times. RNA extraction and qRT-PCR was performed using the QantiTect SYBR Green PCR kit, as described [24]. Gene-specific primers for six endogenous STAT1 target genes as well as for *STAT1* and *GAPDH* were used to amplify the generated cDNAs. The relative expression of a transcript was normalized to the expression of *GAPDH* as determined for each sample. The ΔΔCt-method, based on the formula $2^{-(\Delta Ct\ target - \Delta Ct\ reference\ sample)}$, was used to determine relative expression levels.

2.9. Computational modeling

The kinetic values used in this study are shown in Supplementary Data 1. The system of ordinary differential equations was numerically solved by using the MATLAB software (The MathWorks). Additionally, the Gillespie stochastic simulation algorithm was implemented to test for stochastic effects and to assess the residence time of phosphorylated and unphosphorylated STAT1 in the nucleus. To systematically determine how perturbations in the individual steps of the pathway affect the transcriptional response, we calculated the control coefficients of a response measure X

$$-C_i^X = \frac{p_i}{X}\frac{\partial X}{\partial p_i},$$

where the p_i denote the kinetic parameters. The control coefficients were calculated to describe how much influence a given reaction step has on the STAT1 concentration at steady state. We considered three observables X to characterize the response to a transient IFN-γ stimulus: the response time, the amplitude and the relaxation time of phospho-STAT1 bound to GAS sites. The response time, measured in seconds, is the time the system takes to react to a change in the IFN-γ input, encompassing network latency, signal processing and signal propagation. The amplitude measures the extent of change for a critical parameter when the stimulating IFN-γ is modulated. The relaxation time is defined as the

characteristic time the Jak-STAT1 network takes to return to equilibrium after having been disturbed, where a shorter time indicates a higher speed of recovery and an overall faster relaxation time. Data fitting and statistical analyses of the model parameters were performed as described in Supplementary Data 1.

3. Results

3.1. Experimentally-based modeling of the STAT1 pathway

To access the biological significance of the previously discovered nuclear export block of tyrosine-phosphorylated STAT1, we used a successive interplay of mathematical modeling and experimental

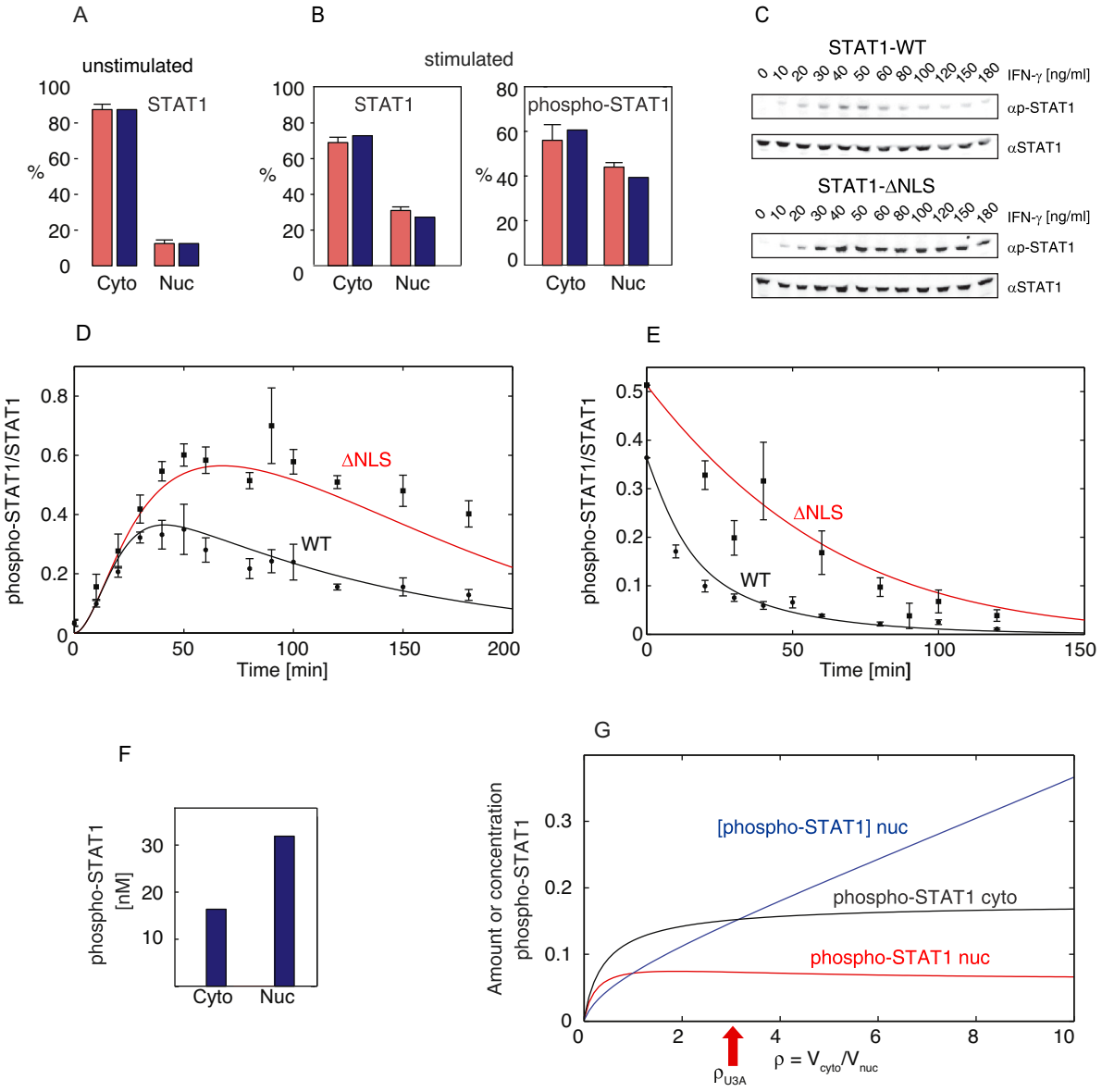

Fig. 2. The mathematical model describes the dynamics of reversible phosphorylation, dimerization and cellular distribution of STAT1 in agreement with experimental data. (A) Nucleocytoplasmic distribution of latent endogenous STAT1 in resting HeLa cells was measured by immunoblotting of nuclear and cytoplasmic extractions, showing means and standard deviations from three independent transfections (red bars). The shuttling rates of latent STAT1 were chosen to reproduce the data with the model (blue bars). (B) Distribution of STAT1 and phospho-STAT1 in IFN-γ-stimulated cells under experimental (red bars) and simulation condition (blue bars). Quantifications of cytoplasmic and nuclear STAT1 pools (total and phospho-STAT1) in fractionated lysates from HeLa cells stimulated for 45 min with IFN-γ (red bars) were used to fit the parameters of the model (blue bars). Histograms indicate means and standard deviations from three independent experiments. (C, D) Phosphorylation kinetics in U3A cells expressing STAT1-WT (circles) or the nuclear import mutant ΔNLS (squares) as measured by immunoblotting with red and black lines, respectively, showing the best fits of the model to the data. The labeling of Y-axis denotes the ratio of phospho-STAT1 to the total cellular STAT1 concentration. Experimental data show means and standard deviations from three independent transfections. (E) Dephosphorylation kinetics measured in STAT1-expressing U3A cells stimulated for 45 min with IFN-γ and subsequently exposed to the kinase inhibitor staurosporine (500 nM) for the indicated times. The red and black lines indicate the best fit of the model. (F) The model simulation of the concentration of phospho-STAT1 in cytoplasm and nucleus (blue bars) shows a two-fold higher concentration in the nucleus although the majority of phospho-STAT1 is cytoplasmic. (G) Nucleocytoplasmic volume difference strongly affects concentration of nuclear STAT1 phosphoprotein. The ratio of STAT1-accessible volumes in cytoplasm and nucleus, $\rho = V_{cyto}/V_{nuc}$, was varied in the model, leaving all other parameters the same. For a continuous IFN-γ stimulus, the steady state values for the amount of phosphorylated STAT1 in cytoplasm (black line) and nucleus (red line) vary little for $\rho > 2$, whereas the nuclear concentration of phospho-STAT1 (blue line) increases almost linearly.

measurements. The mathematical model accounts for the reaction and transport processes that determine the tyrosine phosphorylation and subcellular localization of STAT1 (Fig. 1A, B). The rates of the reaction and transport steps are described by mass-action kinetics (see Supporting Data). Through monitoring the partitioning of microinjected recombinant STAT1 between cytoplasm and nucleus as well as the redistribution of endogenous STAT1 after microinjection of anti-STAT1 antibodies, we determined the half-life for nucleocytoplasmic shuttling of latent STAT1 as ~4 min [4,33]. For these experiments, we injected a STAT1-specific antibody in combination with fluorescently labeled bovine serum albumin as a marker of the injection site into either the nucleus or cytoplasm and, after different time points of incubation, immunocytochemically determined the concentration of the antibody-trapped STAT1 in the injected compartment as well as the depletion of STAT1 in the non-injected compartment. To infer the contributions of energy-independent shuttling and active nuclear export, we quantified the cytoplasmic and nuclear STAT1 fractions in resting HeLa cells prior to cytokine stimulation (Fig. 2A). The rates of tyrosine phosphorylation and dephosphorylation were assessed by means of Western blotting, demonstrating a maximal phospho-STAT1 fraction of 30–35% in both STAT1-expressing Hela cells and STAT1-reconstituted U3A cells under standard stimulation with 5 ng/ml IFN-γ, which resulted in a significant dislocation to the nucleus [26]. We fitted the rate constants determining STAT1 phosphorylation and dephosphorylation simultaneously to time-course measurements of total phospho-STAT1 and the nucleocytoplasmic distributions of intracellular STAT1 pools in stimulated cells (Fig. 2B–D). Both the kinetics of STAT1 phosphorylation and subcellular distribution are quantitatively described by the mathematical model using tightly bound parameters (for details see Supporting Data).

Comparing STAT1-WT and the STAT1-ΔNLS variant that is confined to the cytoplasm due to a disrupted nuclear localization signal [4], we confirmed that phosphatase activity in the nucleus is ~6-fold higher than in the cytoplasm (Fig. 2C, D). Interestingly, even under stimulated conditions, the majority of STAT1 molecules are found in the cytoplasm. However, the concentration of phospho-STAT1 in the nucleus is much higher than in the cytoplasm due to the smaller nuclear volume (Fig. 2F). With the model we were able to study in more detail the dependence of STAT1 activation on the volume ratio between cytoplasm and nucleus ($\rho = V_{cyt}/V_{nuc}$), assuming a fixed total STAT1 concentration in the cell and applying a constant IFN-γ stimulus (Fig. 2G). The total amount of phospho-STAT1 in the nucleus is almost independent of the cytoplasmic-nuclear volume ratio for $\rho > 0.8$, and the concentration of nuclear phospho-STAT1 increases linearly with ρ. As the concentration of activated STAT1 determines the occupancy of the GAS sites (given our estimate of an overall number of $\sim 10^4$ phospho-protein molecules in the nucleus), the volume ratio between cytoplasm and nucleus can affect the rate of gene transcription. Generally, a larger cytoplasm can lead to a higher concentration of phospho-STAT1 in the nucleus and, thus, allows for a more efficient signal transduction.

The STAT1 network can be thought of as consisting of two signaling cycles, an apparently futile cycle of phosphorylation and dephosphorylation in the cytoplasmic compartment, and a functional cycle of phosphorylation, nuclear import, DNA binding, nuclear dephosphorylation and export. The relative importance of the two cycles for the amplitude of phospho-STAT1 in the nucleus depends on the cytoplasmic-nuclear volume ratio. Indeed, we find that the cytoplasmic 'futile' cycle controls the signal amplitude for already moderate $\rho > 1.5$.

Using the Gillespie stochastic simulation algorithm [34], we assessed the residence times of STAT1 molecules in cellular compartments. We found that a STAT1 molecule that enters the nucleus in its tyrosine-phosphorylated state has a mean residence time of 13.1 min (5%–95% CI [confidence interval] = 1.6–48.4 min), before returning to the cytoplasm. For most of this time, namely 12.3 min with a 5%–95% CI ranging from 1.1 to 47.7 min, it is tyrosine phosphorylated. Since the accumulation of STAT1 in the nucleus usually takes several hours, activated STAT1 can shuttle between the two compartments about a dozen times.

The resulting mean time before phospho-STAT1 becomes dephosphorylated after having been imported into the nucleus was determined to be 12.3 min with a 5%–95% confidence interval (5%–95% CI) ranging from 1.1 to 47.7 min. The calculated mean residence time of phospho-STAT1 in the nucleus before it is exported into the cytoplasm was 13.1 min (5%–95% CI = 1.6–48.4 min), indicating that the duration of STAT1 nuclear accumulation, which is in the range of 3 h, is achieved by a combination of short nuclear residence of phospho-STAT1 and high translocation rates.

3.2. Suboptimal signal transmission is required for rapid deactivation

Both the phosphorylation of STAT1 at the plasma membrane (determined by the number of active IFN receptors and the association rate constant) and its binding to GAS sites (determined by the number of accessible sites as well as the respective k_{on} and k_{off}) exert a strong control on the response amplitude (Fig. 3A,B). However, amplitude control is distributed over many processes in the network. In particular, we note that the stability of the phospho-dimers, the dephosphorylation rate in the cytoplasm and the cyto-nucleoplasmic volume ratio ρ all have an appreciable impact on the response amplitude. A qualitatively similar picture is obtained for the response time to an IFN-γ stimulus (Fig. 3C).

The relaxation time after withdrawal of the stimulus is strongly controlled by the parameters of specific DNA binding (number of accessible GAS sites, k_{on} and k_{off}) and the dissociation rate constant of the phospho-dimers (Fig. 3D). The dephosphorylation in the cytoplasm exerts a moderate control, while the contribution of all other steps is much less. Thus, the rate of inactivation of the STAT1 pathway is mainly determined by the dissociation rate of the phospho-STAT1 dimers from the DNA and the dissociation rate of the phospho-dimers themselves. These two processes limit the access of the phosphatases to the activated STAT1.

Remarkably, many parameters exerting a strong control on the relaxation time also have a major impact on the signal strength, such as dissociation of phosphorylated dimers and release from GAS sites, leading to a positive correlation between changes in signal duration and amplitude (Fig. 3B, D). Thus, the pathway operates remote from an optimal signal transmission to ensure fast deactivation after stimulus withdrawal.

3.3. Dimerization protects against noisy signal input and balances efficiency and responsiveness of signaling

The dimerization of STAT1, both before and after tyrosine phosphorylation, is a conspicuous property of the network. By comparing the STAT1 model with a hypothetical network model without dimerizations (and retaining the (de)phosphorylation and nuclear transport reactions), we find that the relative sensitivity to the IFN-γ signal (gain) is strongly decreased in the absence of both types of dimerization (red curve in Fig. 4A). In particular, very small stimuli are suppressed when dimerization is present due to the quadratic dependence of the pathway activity on the concentration of monomeric phospho-STAT1. However, in the absence of dimerization small stimuli would cause pathway activation (Fig. 4A, inset). Therefore, phospho-STAT1 dimerization confers robustness of the pathway against noisy input. To test whether the STAT1 pathway displays the predicted threshold-type response curve (inset of Fig. 4A), we measured the phospho-STAT1 amplitude at different concentrations of IFN-γ. Indeed, we found that the model and data fit each other quantitatively (Fig. 4B).

While the effect of the phospho-dimers on pathway activity is straightforward, the impact of phospho-STAT1 in an antiparallel conformation, which is in equlibium with phospho-STAT1 in a parallel dimer conformation, is less clear. Specifically changing the affinity of this process, we found that tighter N-terminal dimerization tunes down the pathway response. As N-terminal dimers of phosphorylated STAT1

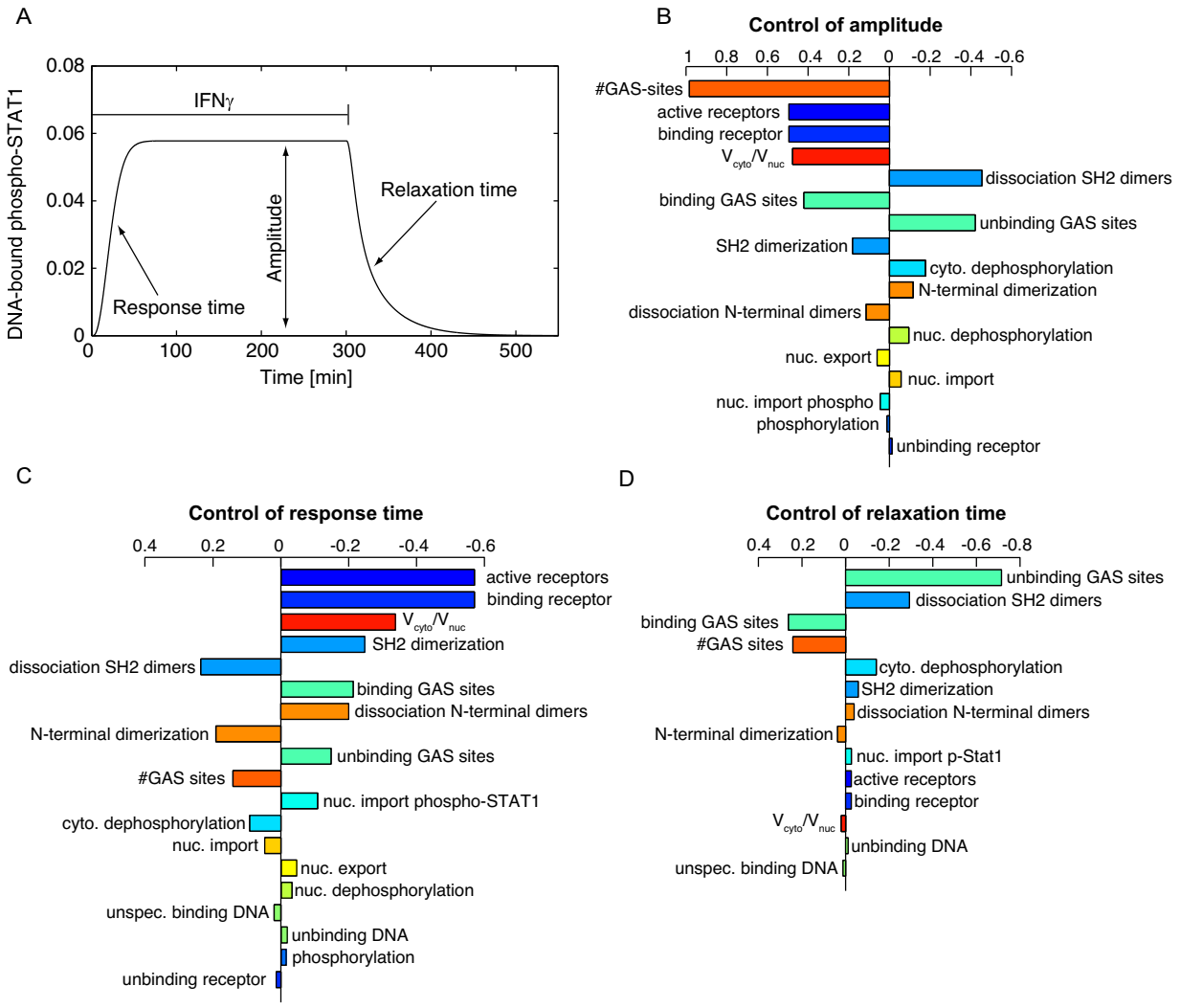

Fig. 3. Control analysis of activation amplitude, response time and relaxation time of the STAT1 pathway. (A) The model was simulated with a representative number ($n = 2000$) of active IFN-γ receptor/Jak complexes until steady state was reached; the system was then allowed to relax to the resting state by setting the number of active IFN receptor/Jak complexes to zero (corresponding to staurosporine application). The time course of DNA-bound phospho-STAT1 in the nucleus was quantified by the amplitude and two characteristic times: the expectation value for reaching the maximum (response time) and for reaching the resting state after withdrawal of the stimulus (relaxation time). The control coefficients for activation amplitude (B), response time (C) and relaxation time (D) were calculated and ranked according to absolute magnitude.

are retained in the cytoplasm, an increased formation of these dimers raises the activation threshold and decreases the signal amplitude by competitive self-interaction.

At first sight, it appears that a tight formation of parallel phospho-dimers would support their rapid nuclear import and, therefore, be beneficial for the efficiency of signal transduction. Indeed, the amplitude of nuclear phospho-STAT1 and thus the occupancy of GAS sites increases with the affinity of phosphotyrosine-SH2 domain dimerization (Fig. 4C). However, there is a price to be paid for this efficiency in terms of the regulation of the pathway because tight phospho-dimers are protected from dephosphorylation and would persist even after the interferon stimulus has subsided. Consequently, the relaxation of the pathway is strongly retarded by very high affinity of phosphotyrosine-SH2 domain dimerization (Fig. 4D). Therefore, the affinity must be such that a trade-off between efficient activation and rapid responsiveness of the pathway to changing input stimuli is achieved.

The model shows that a further decrease of the K_d value from its measured value (50 nM) could make signal transduction considerably more efficient (Fig. 4C), but concomitantly makes the pathway less sensitive to changes in signal input because the duration of the signal is prolonged. This suggests that affinity of phosphotyrosine-SH2 domain dimerization may realize the predicted compromise between efficiency and responsiveness.

3.4. Enhanced nuclear localization of STAT1 disrupts pathway functionality

To test the validity of the model experimentally, we examined the effect of perturbations of the network design. We tested the effect of enhanced localization of STAT1 in the cell nucleus by adding NLS sequences of different strengths to a STAT1 fusion protein tagged with green fluorescent protein (STAT1-GFP). Strongly and weakly import-enhanced STAT1 variants (STAT1-sNLS and STAT1-wNLS) were obtained by using a tandem arrangement of the native NLS (PKKKRKVE) from the large T antigen of SV40 and an attenuated version of it (PKKKAKVE), respectively.

The different strengths of the NLS constructs became apparent by assaying the subcellular STAT1 localization in resting cells using fluorescence microscopy (Fig. 5A). In contrast to STAT1-WT, displaying a nearly pancellular resting distribution, STAT1-wNLS and STAT1-sNLS

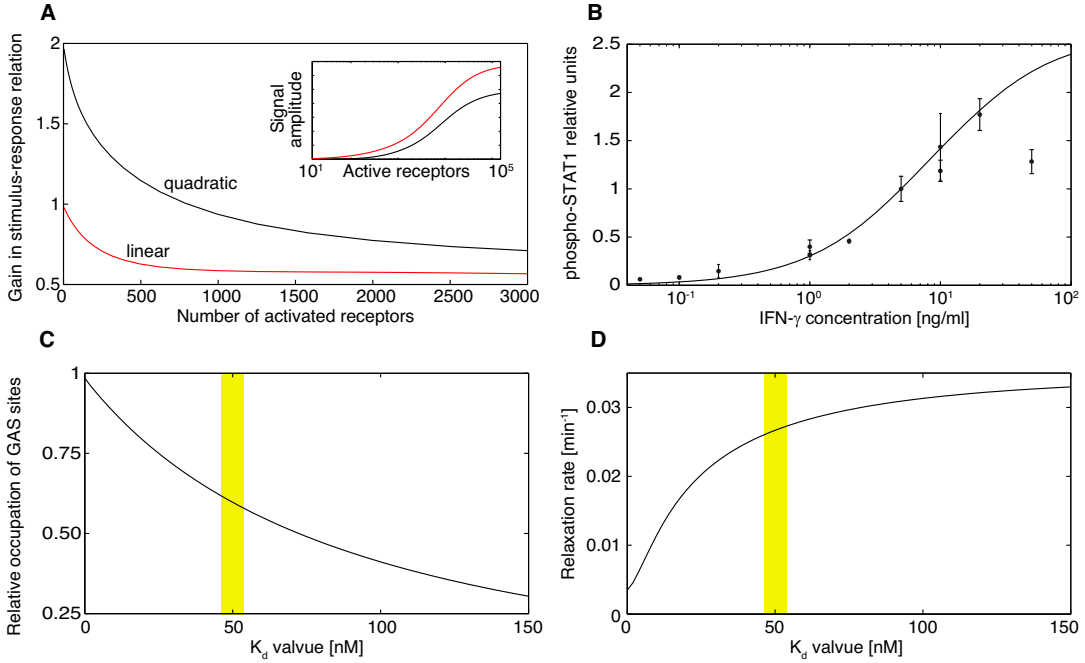

Fig. 4. Effects of STAT1 dimerization on signal transduction. (A) Dimerization results in a higher gain in the stimulus-response relation, as seen by comparing the gain of the model with STAT1 dimerization (black line) to a hypothetical linear model without dimerization (red line). Moreover, STAT1 dimerization causes a sharper response threshold than seen in the hypothetical model (inset). Specifically, the dimerization step of phospho-STAT1 suppresses network activation by subthreshold stimuli. (B) Phospho-STAT1 levels in reconstituted U3A cells treated for 45 min with different concentrations of IFN-γ as determined experimentally by immunoblotting (shown are means and standard deviations). By varying the IFN-γ stimulus in the simulations, a dose-response curve for the model was calculated, using the stimulation with 5 ng/ml IFN-γ as a reference point (black curve). (C) Predicted occupancy of GAS sites versus dissociation rate constant of phosphotyrosine-SH2 domain dimerization. (D) Predicted relaxation rate (defined as the inverse relaxation time of the system) versus dissociation rate constant of phosphotyrosine-SH2 domain dimerization. A higher stability of the phospho-dimer would cause a stronger signal but would also strongly retard relaxation after withdrawal of the IFN-γ stimulus.

showed a preferentially nuclear localization with stronger nuclear accumulation of STAT1-sNLS. As a control, a mutant with an added permutated NLS sequence (PKEAKVKK), termed STAT1-LSN, exhibited the same pancellular resting distribution as the WT protein.

Upon stimulation with IFN-γ, the wNLS and LSN variants accumulate in the nucleus to the same degree as WT STAT1, while the already strong nuclear accumulation of the sNLS variant is not further augmented by IFN-γ treatment. However, the phosphorylation level is decreased in the wNLS and sNLS variants with enhanced nuclear import according to the strength of the additional NLS (Fig. 5B, C). Even the sNLS construct, which appears to be completely localized in the nucleus already in resting cells, became phosphorylated, albeit to a lesser extent as the WT protein. This observation implies that, like the WT protein, both NLS mutant proteins cycle between the cytoplasm and the nucleus and thus have access to the IFN-γ receptor/Jak complex at the plasma membrane. Application of the kinase inhibitor staurosporine caused a rapid decline of STAT1 phosphorylation, showing that the maintenance of phosphorylation requires continuous Jak activity (Fig. 5B, C).

We calculated the mutant phenotypes in the model by augmenting the nuclear import rate constants for both STAT1 phospho-dimers and the unphosphorylated protein. The nuclear presence of the protein under resting and stimulated conditions increases with the degree of import acceleration, while the phosphorylation levels decrease (Fig. 5D). These results -are in line with the corresponding experimental data. To test whether the phenotype of the STAT1-NLS variants is due to enhanced import of latent STAT1 and/or the phospho-protein, we simulated separate increases of the import rates of the two subspecies. As shown in Fig. 5D, accelerated import of latent STAT1 alone yields the same behavior, whereas the WT behavior is fully retained when the import of phospho-STAT1 is accelerated. To confirm that the NLS variants displayed normal DNA binding kinetics, we performed competition gelshift experiments in the presence of a 750-fold molar excess of unlabeled GAS elements (Fig. 5E). Given the unaltered dissociation kinetics from a high-affinity GAS binding element, we ruled out the hypothesis that the predominant nuclear distribution resulted from an abnormal DNA binding. The impaired nuclear export of the wNLS and sNLS variants not only resulted in their decreased tyrosine phosphorylation (Fig. 5B, C) but was also associated with a significantly reduced reporter gene activation, as demonstrated in Fig. 5F. In summary, our data show that the phosphorylation rate can be strongly regulated by the velocity of nuclear import of latent STAT1. This is the case because the rapid nuclear import of latent STAT1 competes with its activation by the Jak kinases.

3.5. *Nuclear retention of phosphorylated STAT1 enhances efficiency and responsiveness of signal transduction*

As we have previously shown, the nuclear export is restricted to the unphosphorylated form of the protein [16]. To enhance nuclear export, we generated a STAT1 construct by adding the STAT1-specific nuclear export signal sequence located in the DNA-binding domain heterotopically to the C-terminus of the protein (STAT1-NES; [23]). Using GFP-tagged STAT1-WT and the NES variant, we confirmed that resting cells showed a cytoplasmic localization of STAT1-NES that contrasts with the pancellular distribution of STAT1-WT. Treatment of the cells with leptomycin B (LMB), a potent inhibitor of the exportin Crm1 [35], inhibited the enhanced nuclear export and resulted in a pancellular distribution of STAT1-NES in resting cells [24]. Therefore, unphosphorylated STAT1-NES, like the WT protein, shuttles continuously in and out of the nucleus, but in the absence of LMB with a higher export rate than STAT1-WT. Upon stimulation with IFN-γ, STAT1-NES did not accumulate in the nucleus, despite its strong tyrosine phosphorylation

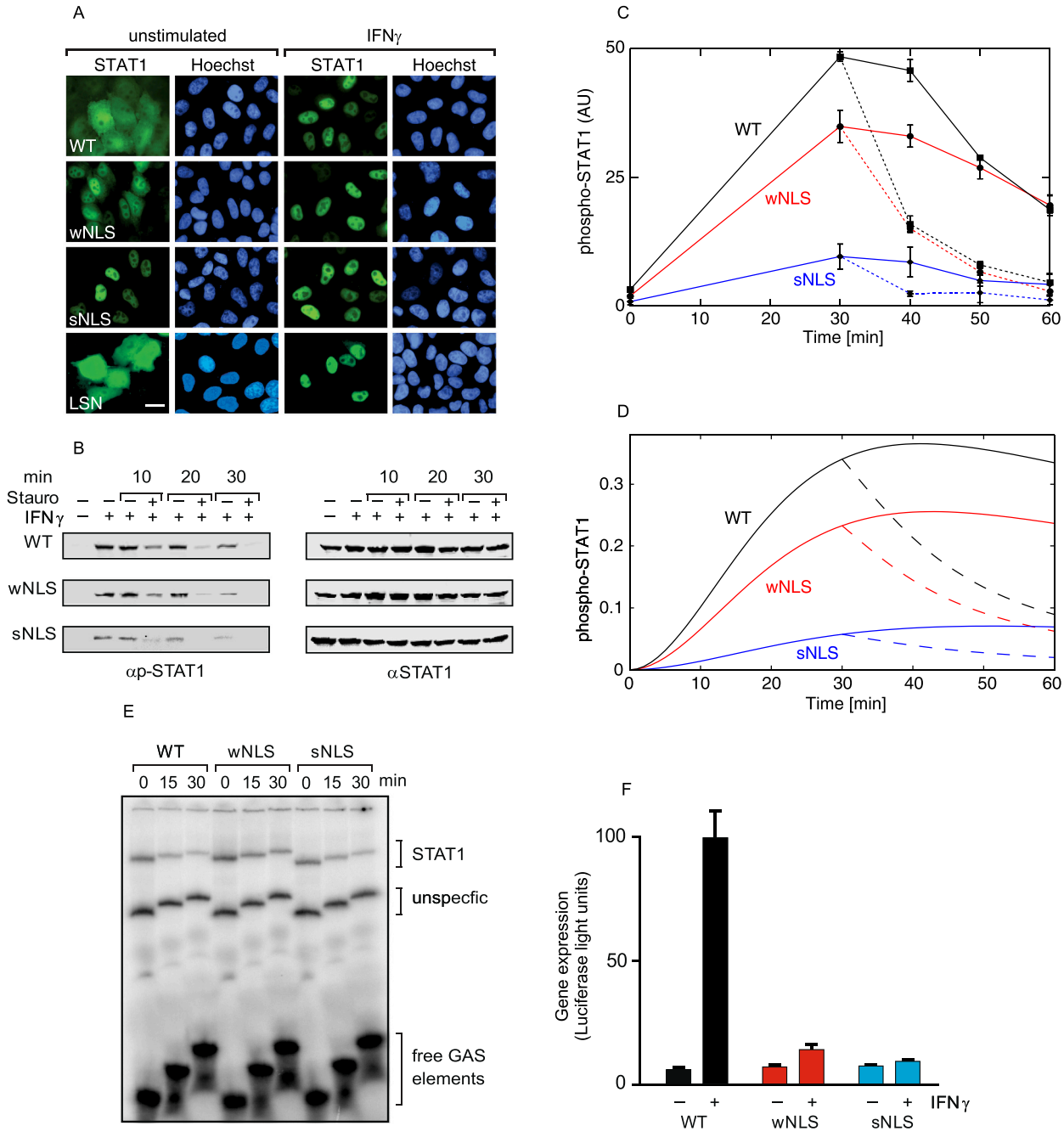

Fig. 5. Enhanced nuclear import of STAT1 reduces cytokine-induced tyrosine phosphorylation. (A) The addition of nuclear localization signals (NLSs) of different strengths to STAT1-GFP resulted in a gradual increase of nuclear STAT1 in resting cells and practically unaltered nuclear accumulation upon cytokine stimulation. HeLa cells were transiently transfected with plasmids coding for GFP fusions of wild-type STAT1 (WT), the weak import mutant (wNLS), the strong import mutant (sNLS), and a mutant with a permutated NLS sequence thereof (LSN). Resting cells and cells stimulated for 1 h with IFN-γ were fixed, stained for DNA (Hoechst) and processed for the microscopic detection of GFP fluorescence (scale bar: 20 μm). (B, C) Both STAT1 import variants wNLS and sNLS exhibit reduced but detectable phosphorylation levels upon IFN-γ stimulation and are sensitive to the kinase inhibitor staurosporine. Cells were stimulated for 30 min with 5 ng/ml IFN-γ and then incubated further in the absence (full lines) or presence of 500 nM staurosporine (dotted lines), respectively. Western blots using whole-cell extracts from transfected U3A cells expressing either wild-type STAT1-GFP (WT), STAT1-wNLS or STAT1-sNLS (B) were quantified from three independent experiments (C). (D) Model simulations reproduce the observed decreases in STAT1 phosphorylation with import enhancement (implemented by increasing the import rate constants by 0.2 min^{-1} and 2 min^{-1} for STAT1-wNLS and STAT1-sNLS, respectively). (E) Autoradiogram from a competition gelshift experiment using STAT1-reconstituted U3A whole cell extracts expressing WT or mutant STAT1 with a weak (wNLS) or strong (sNLS) NLS. The extracts from IFN-γ-pretreated cells were first incubated with [^{33}P]-labeled GAS elements (M67) and subsequently exposed to a 750-fold excess of unlabeled M67 as competitor for 0, 15, and 30 min. The unchallenged reactions (0 min) were first loaded on the running polyacrylamide gel, while reactions from 30 min time point were loaded last, which resulted in their stepwise migration pattern on the gel. Note that the NLS variants display similar dissociation kinetics from GAS elements as the WT protein, ruling out the possibility that they function as DNA-binding mutants. (F) The NLS variants display reduced transcriptional activity. STAT1-negative U3A cells were transfected with the indicated STAT1 expression plasmids coding for GFP-tagged fusion proteins in combination with the luciferase reporter gene construct 3xLy6E and a constitutively expressed β-galactosidase plasmid used for normalization. Cells were stimulated with 50 ng/ml of IFN-γ for 0 h (−) or 6 h (+) before extracts were tested for luciferase and β-galactosidase production.

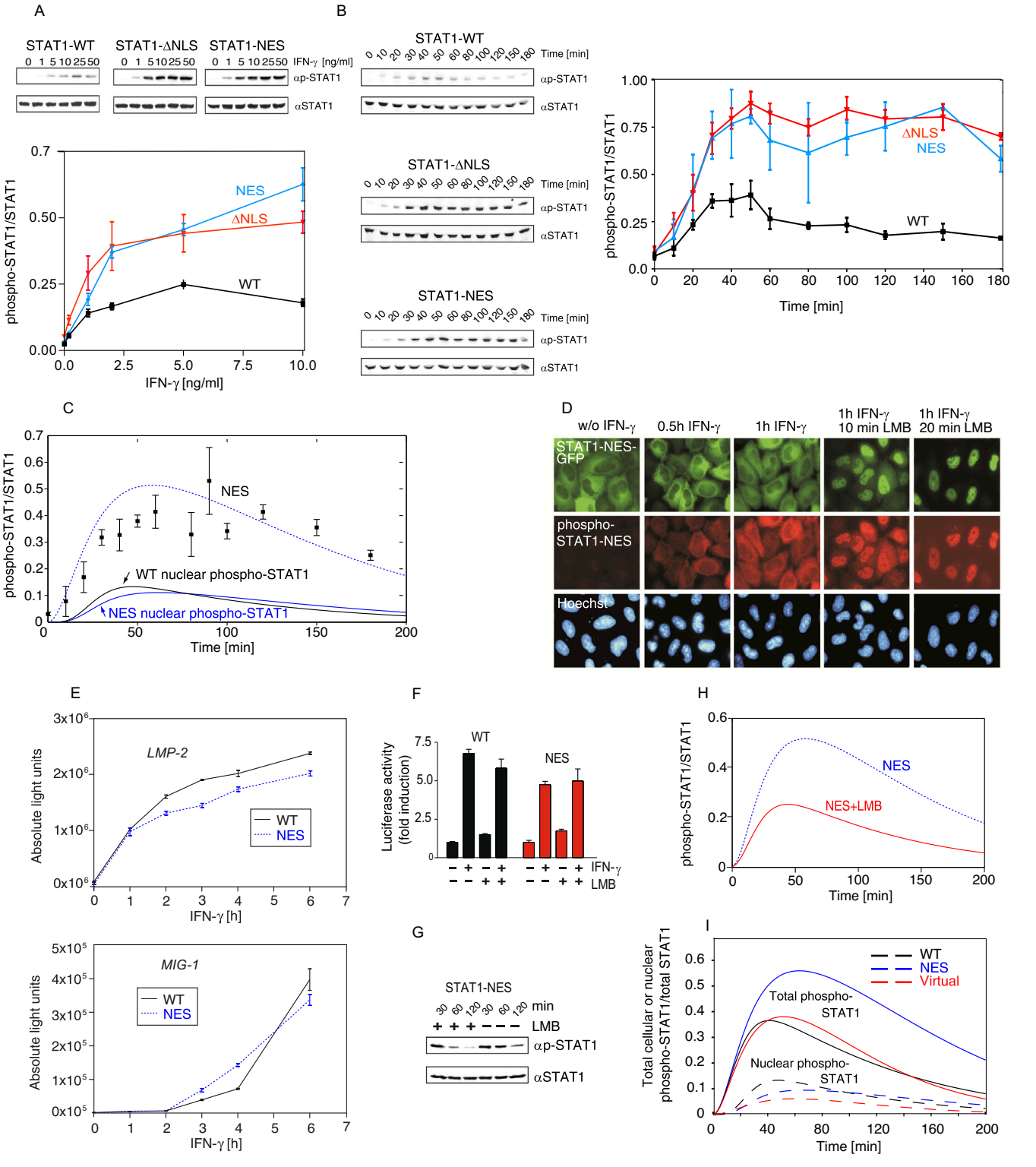

(caption on next page)

Fig. 6. Effect of accelerated nuclear export of STAT1 on subcellular distribution, cytokine-induced tyrosine phosphorylation, and target gene transcription. (A) Elevated tyrosine phosphorylation of the STAT1 export mutant NES and the dimer-specific import mutant ΔNLS. Shown are Western blot results and the quantification thereof from cellular extracts of HeLa cells expressing GFP fusion proteins of STAT1-WT, -NES, and -ΔNLS treated with increasing concentrations of IFN-γ, as indicated ($n = 3$). (B) Prolonged and enhanced phosphorylation of both STAT1-NES and ΔNLS as compared to the wild-type protein. U3A cells expressing the respective STAT1 variants were stimulated with IFN-γ for the indicated times (0–180 min). Western blots were prepared from whole-cell extracts, probed with a STAT1-specific phosphotyrosine antibody and reprobed with a STAT1 antibody (n = 3). (C) The phosphorylation kinetics of the NES variant were simulated with the model (blue line) and compared to the quantification of the data in (B). The additional export rate of STAT1-NES was deduced from the nucleocytoplasmic distribution in resting cells. The model predicts no significant difference in nuclear phospho-STAT1 between STAT1-NES (blue line) and wild-type STAT1 (black line). (D) Fluorescence microscopy demonstrating the kinetics of tyrosine phosphorylation and nuclear accumulation of STAT1-NES-GFP in U3A cells treated with IFN-γ and subsequently exposed to leptomycin B (LMB) for the indicated times. Fixed cells were stained with an antibody specifically recognizing tyrosine-phosphorylated STAT1 followed by a Cy3-labeled secondary antibody. Micrographs show the localization of STAT1-GFP (first row), phosphorylated STAT1 (second row) and the corresponding Hoechst-stained nuclei (third row). (E) In agreement with the predicted similar phospho-STAT1 levels in the nucleus, the induction of STAT1 target genes by STAT1-NES and STAT1-WT is very similar both for late and early induced targets. Transcript levels were determined by reverse transcriptase-PCR. (F) Representative results from a reporter gene assay in transfected U3A cells expressing WT or the NES variant in the absence or present of IFN-γ and/or LBM, as indicated. (G) Inhibiting Crm1-dependent nuclear export results in a more rapid decline of STAT1-NES phosphorylation, as determined by Western blots of whole-cell extracts. STAT1-NES-expressing U3A cells were treated for 45 min IFN-γ in the presence or absence of LMB. (H) Simulating LMB and staurosporine treatment with the model yielded a reduced and shortened phosphorylation of STAT1-NES that matches the experimental observation. (I) Modeling of a virtual system mutant with abrogated nuclear export block of phospho-STAT1 demonstrates reduced concentrations of nuclear STAT1, despite normal overall phosphorylation kinetics, which is in contrast to the STAT1-NES mutant described above. Solid lines indicate cellular phospho-STAT1 to total cellular STAT1 ratios, while dashed lines indicated the nuclear phospho-STAT1 to the total cellular STAT1 level.

(Fig. 6A–C). However, nuclear accumulation of the STAT1-NES variant in IFN-γ-treated cells was restored after 10 min of exposure to LMB (Fig. 6D). These findings showed that although phosphorylated STAT1-NES was imported into the nucleus, the presence of the heterotopic export signal prevented sufficient nuclear build-up. These data confirm that phospho-STAT1-NES enters the nucleus, but cannot be retained there due to its rapid export as a phosphoprotein [24]. This conclusion is further corroborated by the comparison with the STAT1-ΔNLS variant, which is not imported into the nucleus as a phosphoprotein and, consequently, its nuclear accumulation cannot be induced by any of the protocols used (data not shown).

The hyper-phosphorylation of STAT1-NES in response to an IFN-γ stimulus was similar to the enhanced phosphorylation observed for the STAT1-ΔNLS variant (Fig. 6A, B). This finding suggested a predominantly cytoplasmic localization of STAT1-NES and STAT1-ΔNLS (with access to the Jak kinases and exposure to comparatively weak phosphatase activity) as the main cause of their hyperphosphorylation.

To model the STAT1-NES construct, we estimated the increased nuclear export rate due to the heterotopic NES sequence from the STAT1-NES distribution in resting cells. We assumed the same additional export rate constant for all nuclear STAT1 species (phosphorylated and unphosphorylated, dimeric and monomeric) as the added NES sequence is unlikely to be regulated by phosphorylation and/or dimerization. With this modification, the model reproduces quantitatively the measured phosphorylation time course (Fig. 6C). While IFN-γ stimulation alone did not trigger nuclear retention of the NES variant, a 10-min exposure to LMB in the IFN-γ-pretreated restored the inhibited nuclear accumulation (Fig. 6D). Unexpectedly, the model predicts that the phospho-STAT1-NES fraction in the nucleus is very similar to STAT1-WT. To test this prediction, we monitored the induction kinetics of STAT1 target genes after IFN-γ stimulation in STAT1-NES-expressing cells and, indeed, found no significant difference to STAT1-WT (Fig. 6E, Supplemental Data 2). Despite a strikingly different nuclear accumulation behavior as compared to the WT protein, the pattern of reporter gene activation for the NES construct is quite similar to the WT protein (Fig. 6F). This finding confirms that shuttling between the two cellular compartments constitutes a crucial feature of this signal pathway. Even a variant with a hyperactive export and consequent failure to accumulate in the nucleus induces cytokine-dependent genes to an extent similar to the WT protein.

Moreover, the model of the NES variant also reproduces the weaker phosphorylation observed in the presence of LMB to block active nuclear export (Fig. 6F–H). The model indicates that LMB reduces STAT1-NES phosphorylation due to two effects: (i) the nuclear retention subjects the phospho-dimer to the nuclear phosphatases rather than the lower-activity cytoplasmic phosphatases; and (ii) the decreased export rate of unphosphorylated STAT1-NES retards its (re-)phosphorylation. Thus, the mathematical model reproduces the phenotype of the STAT1-NES simply by enhancing the nuclear export rate of latent STAT1. Remarkably, the transcriptional response of the STAT1 pathway is robust against an enhancement of the STAT1 nuclear export rate, including the unphysiological export of the phospho-protein.

Finally, we modeled a virtual mutant, which is not subjected to the nuclear export block of phospho-STAT1. This mutant displays free shuttling of phosphorylated STAT1 dimers between the nucleus and the cytoplasm without generally increased export rates. While an experimental approach for such a mutant is currently not feasible, its mathematical simulation allowed us to estimate the physiological consequence of a disrupted network design by abrogating nuclear retention of phospho-STAT1. In contrast to the experimentally tested NES variant, this virtual mutant displayed no evidence of hyperphosphorylation, but instead showed normal kinetics of tyrosine phosphorylation upon stimulation of cells with IFN-γ (Fig. 6I). While the total amount of intracellular phospho-STAT1 was indistinguishable from the WT molecule, the system mutant showed considerably lower nuclear concentrations of activated STAT1 throughout the entire stimulation period than its WT counterpart. Thus, coupling of nuclear export to its prior dephosphorylation is a simple mechanism for increasing the concentration of STAT1 phospho-dimers in the nucleus and, possibly also, for the initiation of transcriptional events.

4. Discussion

Using an interplay of quantitative experimentation and mathematical modeling, we investigated the biological significance of nuclear retention of phosphorylated STAT1 and defined its control on the function as a transcriptional activator. Our data clearly support the hypothesis that the previously defined nuclear export block of phospho-STAT1 constitutes a fundamental design principle for the STAT1 network. Computational analysis uncovered three crucial processes that control the nuclear accumulation of transcriptionally active, tyrosine-phosphorylated STAT1 following ligand binding to the cytokine receptor: the kinetics at GAS sites, the stability of the phosphotyrosine-SH2 dimers, and the enzymatic phosphatase activities. With respect to all other parameters, the system behavior is comparatively robust. In contrast to these rate-limiting steps, the import of phospho-STAT1 dimers into the nucleus has much less control. The supply of dephosphorylated STAT1 molecules in the cytosol after their nuclear exit remains the critical transition step that determines the rate of cytoplasmic re-activation. As expected, the number of active receptor complexes and their binding kinetics achieve a significant positive control on the level of nuclear phospho-STAT1 concentrations. In contrast, the

nuclear import rate of the phosphorylated molecule has little kinetical control on shaping the signal amplitude, suggesting that modulating the transport velocity of the unphosphorylated STATs rather than of the phospho-dimer might have evolved as a putative control mechanism for regulating the strength of cytokine signaling. However, the underlying molecular mechanisms that modulate transport kinetics have not been systematically investigated so far [36–38].

Interestingly, nuclear accumulation is dispensable for gene activation, since also the STAT1-NES variant, that completely lacks nuclear build-up as judged by fluorescence microscopy, displays strikingly normal gene activation. Thus, for transcription of cytokine-inducible genes only small amounts of intranuclear STAT1 phospho-dimers are required, while the majority of nuclear STAT1 does not contribute to promoter binding. This implies that phospho-STAT1 is retained predominantly outside GAS sites on non-specific DNA sequences. This finding is in line with previous data that there is a kinetically determined inactivation of STAT1 dimers depending on the sequence-specific dissociation rate from DNA [24].

The impaired shuttling of the STAT1-NLS constructs clearly demonstrates that the balance between nuclear import and export, rather than unidirectional translocation, regulates signal strength and duration, suggesting that the biological strengths of both the NES sequence functioning exclusively for non-phosphorylated STAT1 and the dimer-specific NLS have co-evolved. Therefore, it is proposed that the STAT1 cycle linking biological functions of unphosphorylated and phosphorylated variants within one single design network is a hallmark of STAT1-regulated signal processing. The rapid break-down of nuclear accumulation following kinase inhibition suggests that under physiological conditions the cycling time of endogenous STAT1 molecules is very short and does not exceed 20 min. The half-lives of nuclear import of tyrosine-phosphorylated STAT1, as well as of the constitutive nucleo-cytoplasmic translocation of unphosphorylated STAT1, were predicted to be similarly short in our model shown here, which closely agrees with the reported half-lives of activated STAT5 (≈5 min) and STAT6 (≈6 min), respectively [39,40].

According to our model, one function of phosphotyrosine/SH2 domain dimerization is suppression of signal propagation at low signal input (Fig. 4A). This effect is amplified by the cytoplasmic phosphatase activity. For very small amounts of phospho-STAT1 in the cytoplasm, the probability of binding to the phosphatase is higher than binding to another phospho-STAT1 molecule, thereby preventing nuclear import and induction of gene transcription. In the hypothetical case of a model, where STAT1 does not form phospho-dimers, even small stimuli would cause pathway activation. Dimerization appears to set an activation threshold that confers robustness of the pathway against noisy input. Enhancing the stability of phosphotyrosine-SH2 dimers favours binding to GAS sites at the price of signal control, since tight phospho-dimers bound to DNA are protected from dephosphorylation and prolong signal duration even after the interferon stimulus has subsided. Consequently in this case, the relaxation of the pathway is strongly retarded (Fig. 4D). Therefore, the measured K_d value in the range of 50 nM [26] appears to be a compromise between efficient activation and rapid responsiveness to changing input stimuli.

The enhanced activation level of a STAT1 variant with hyper-physiological nuclear export reveals that the STAT1 signaling network is not designed for maximal signal strength. It appears that the WT molecule more closely follows changes in the ligand-induced receptor occupation as compared to the STAT1-NES version with accelerated export activity, indicating that the coupling between receptor-based and transcriptional processes is stringently regulated through the network topology. Enhancing the export velocity promotes signal persistence, instead of the rapid decline that normally follows withdrawal of stimulus application, and critically impairs the ability of STAT1 to rapidly switch from latent to transciptionally active states. The regulatory control of a physiological NES strength, however, as in the WT protein, ensures that the information flow input is translated into a substantial, but also dynamic signal response that follows changes in extracellular stimuli without long delay. A similar phenotype has been described for pathogenic STAT1 gain-of-function mutations causing chronic mucocutaneous candidiasis, which shift the equlibrium from the antiparallel to the parallel dimer formation [41–44].

Although a STAT1 mutant with accelerated nuclear export fails to produce a noticeable nuclear accumulation following interferon exposure, the model shows that the intranuclear concentration of phosphorylated STAT1 is essentially identical to the WT protein (Fig. 6C). This finding is in good agreement with our experimental data demonstrating that the time course of transcriptional activity of the hyperactive export mutant closely resembles that of its WT counterpart for six endogenous target genes. Nevertheless, without retention of the phospho-STAT1 in the nucleus, the deactivation kinetics of the pathway is slower and higher phosphorylation levels are achieved. Thus, the retention of phospho-STAT1 to the nucleus renders the pathway response faster and more efficiently. However, as the subcellular distribution of both variants differs dramatically in response to cytokine exposure, potential cytoplasmic functions of STAT1 protein that are independent of cytokine stimulation and exerted by the unphosphorylated molecule may be critically altered.

In order to elucidate the physiological significance of the previously described nuclear export block of tyrosine-phosphorylated STAT1 [16], we finally used our validated set of kinetic rate equations to simulate a virtual mutant with abrogated nuclear retention of phosphorylated STAT1. Modeling this system mutant allowed us to test for the consequences of an uncoupling of nuclear export from dephosphorylation, which can currently not be examined by means of established biochemical experimentation. Interestingly, we found that although the overall phosphorylation rate of this mutant is not disturbed, the concentration of phospho-STAT1 within the nucleus is nevertheless significantly reduced upon stimulation of cells with cytokines. This striking finding underlines the central role of the inherent network design of the STAT1 signaling circuit, in which nuclear export is mechanistically linked to prior inactivation by tyrosine phosphatases.

When describing our model in terms of relevant transition steps, we did not take feedback regulation through inhibitory proteins into account. Proteins such as suppressor of cytokine signaling 1 (Socs1), that are under transcriptional control of STAT1 transcription factors, have been reported to negatively affect cytokine signaling. However, their effect in damping signal amplification is not addressed in the model presented and thus needs further investigation [45–47]. Additionally, we did not consider alterations in receptor dynamics including internalization or proteolytic degradation of cytokine receptors, because of the low affinity of STAT1 molecules for activated cytokine receptors [48]. Putative biological functions of the unphosphorylated STAT1 molecule in either the cytosol or the nucleus, such as induction of apoptosis or interaction with other transcription factors, were also not addressed in our model [49,50]. Therefore, the complex spatiotemporal regulation of the pathway including the interaction with regulatory proteins needs further research efforts that are far beyond the STAT1 core module described here for IFN-γ-mediated signal transduction.

In an important publication, Klingmüller and colleagues previously identified molecular mechanisms that regulate the sensitization of IFN-α signaling in hepatocytes [51]. This leads to the formation of a STAT1: STAT2 heterodimer bound to interferon response factor 9 (IRF9), a complex also known as interferon-stimulated gene factor 3 (ISGF3). Combined with an earlier report from the same laboratory containing data on the Jak2/STAT5 core module [51,52], these approaches underscore the scientific utility of mathematical simulations in investigating complex signal transduction pathways that integrate extracellular and intracellular signals to generate appropriate cytokine-driven responses.

An important limitation of our experimental design is the use of GFP-tagged fusion proteins for direct fluorescence staining in an over-expressing transfection setting. In a previous publication, we showed

that GFP tagging decreases the nucleocytoplasmic shuttling rate specifically of the unphosphorylated STAT1 protein resulting in reduced transcriptional activity [53]. Despite unimpaired nuclear import of activated phospho-STAT1, GFP-based labeling techniques may considerably underestimate the actual shuttling rate of unphosphorylated native STAT1. Furthermore, the model prediction that the nuclear concentration of the NES mutant is only slightly reduced compared to the WT molecule requires future experimental validation.

In summary, our data presented reveal how the inherent dynamic properties of the STAT1 signaling circuit contribute to signal specificity. The balanced strength of the autochthonal NES and NLS sequences within the STAT1 molecule ensures real-time coupling of receptor-based and transcriptional processes at the expense of signal amplification. Although the pathway operates far from optimal signal output, its unique design features facilitate a high degree of adaptability allowing for a prompt and, nevertheless, efficient response to a changing extracellular environment.

CRediT authorship contribution statement

Thomas Meyer: Writing – review & editing, Writing – original draft, Validation, Supervision, Methodology, Formal analysis, Data curation, Conceptualization. **Florian Lamprecht:** Writing – review & editing, Validation, Software, Methodology, Investigation, Formal analysis, Data curation. **Andreas Begitt:** Writing – review & editing, Methodology, Investigation, Formal analysis, Data curation, Conceptualization. **Thomas Höfer:** Writing – review & editing, Writing – original draft, Validation, Supervision, Project administration, Investigation, Funding acquisition, Formal analysis, Data curation, Conceptualization. **Uwe Vinkemeier:** Writing – review & editing, Visualization, Validation, Supervision, Resources, Funding acquisition, Formal analysis, Data curation, Conceptualization.

Consent for publication

Not applicable.

Ethics approval and consent to participate

Not applicable.

Declaration of Generative AI and AI-assisted technologies in the writing process

The authors declare that during the preparation of this manuscript, they used OpenAI GPT-5 Chat for the purpose of correct language spelling. The authors subsequently reviewed and edited the content as necessary and assume full responsibility for the accuracy and integrity of the published work.

Funding

Open Access funding enabled and organized by the German Projekt DEAL. The research was funded by institutional grants to TH and UV.

Declaration of competing interest

The authors declare that they have no conflict of interest.

Acknowledgements

Not applicable.

Appendix A. Supplementary data

Supplementary data to this article can be found online at https://doi.org/10.1016/j.bbagrm.2026.195151.

Data availability

Data will be made available on request.

References

[1] R.L. Philips, Y. Wang, H. Cheon, Y. Kanno, M. Gadina, V. Sartorelli, C.M. Horvath, J.E. Darnell Jr., G.R. Stark, J.J. O'Shea, The JAK-STAT pathway at 30: much learned, much more to do, Cell 185 (21) (2022) 3857–3876.
[2] R.P. Agashe, S.M. Lippman, R. Kurzrock, JAK: not just another kinase, Mol. Cancer Ther. 21 (12) (2022) 1757–1764.
[3] F. Perner, H.L. Pahl, R. Zeiser, F.H. Heidel, Malignant JAK-signaling: at the interface of inflammation and malignant transformation, Leukemia 39 (5) (2025) 1011–1030.
[4] T. Meyer, A. Begitt, I. Lödige, M. van Rossum, U. Vinkemeier, Constitutive and IFN-γ-induced nuclear import of STAT1 proceed through independent pathways, EMBO J. 21 (3) (2002) 344–354.
[5] R. Zeng, Y. Aoki, M. Yoshida, K. Arai, S. Watanabe, Stat5B shuttles between cytoplasm and nucleus in a cytokine-dependent and -independent manner, J. Immunol. 168 (9) (2002) 4567–4575.
[6] A.L. Pranada, S. Metz, A. Herrmann, P.C. Heinrich, G. Müller-Newen, Real time analysis of STAT3 nucleocytoplasmic shuttling, J. Biol. Chem. 279 (15) (2004) 15114–15123.
[7] D. Boehmer, I. Zanoni, Interferons in health and disease, Cell 188 (17) (2025) 4480–4504.
[8] T. Sekimoto, N. Imamoto, K. Nakajima, T. Hirano, Y. Yoneda, Extracellular signal-dependent nuclear import of Stat1 is mediated by nuclear pore-targeting complex formation with NPI-1, but not Rch1, EMBO J. 16 (23) (1997) 7067–7077.
[9] R. Fagerlund, K. Mélen, L. Kinnunen, I. Julkunen, Arginine/lysine-rich nuclear localization signals mediate interactions between dimeric STATs and importin α5, J. Biol. Chem. 277 (33) (2002) 30072–30078.
[10] K.M. McBride, G. Banninger, C. McDonald, N.C. Reich, Regulated nuclear import of the STAT1 transcription factor by direct binding of importin-α, EMBO J. 21 (7) (2002) 1754–1763.
[11] J. Nardozzi, N. Wenta, N. Yasuhara, U. Vinkemeier, G. Cingolani, Molecular basis for the recognition of phosphorylated STAT1 by importin α5, J. Mol. Biol. 402 (1) (2010) 83–100.
[12] R.L. Haspel, M. Salditt-Georgieff, J.E. Darnell Jr., The rapid inactivation of nuclear tyrosine phosphorylated Stat1 depends upon a protein tyrosine phosphatase, EMBO J. 15 (22) (1996) 6262–6268.
[13] R.L. Haspel, J.E. Darnell Jr., A nuclear protein tyrosine phosphatase is required for the inactivation of Stat1, Proc. Natl. Acad. Sci. U. S. A. 96 (18) (1999) 10188–10193.
[14] T. Tenev, S.A. Böhmer, R. Kaufmann, S. Frese, T. Bittorf, T. Beckers, F.D. Böhmer, Perinuclear localization of the protein-tyrosine phosphatase SHP-1 and inhibition of epidermal growth factor-stimulated STAT1/3 activation in A431 cells, Eur. J. Cell Biol. 79 (4) (2000) 261–271.
[15] J. ten Hoeve, M. de Jesus Ibarra-Sanchez, Y. Fu, W. Zhu, M. Tremblay, M. David, K. Shuai, Identification of a nuclear Stat1 protein tyrosine phosphatase, Mol. Cell. Biol. 22 (16) (2002) 5662–5668.
[16] T. Meyer, A. Marg, P. Lemke, B. Wiesner, U. Vinkemeier, DNA binding controls inactivation and nuclear accumulation of the transcription factor Stat1, Genes Dev. 17 (16) (2003) 1992–2005.
[17] K.M. McBride, C. McDonald, N.C. Reich, Nuclear export signal located within the DNA-binding domain of the STAT1 transcription factor, EMBO J. 19 (22) (2000) 6196–6206.
[18] A. Marg, Y. Shan, T. Meyer, T. Meissner, M. Brandenburg, U. Vinkemeier, Nucleocytoplasmic shuttling by nucleoporins Nup153 and Nup214 and CRM1-dependent nuclear export control the subcellular distribution of latent Stat1, J. Cell Biol. 165 (6) (2004) 823–833.
[19] A. Begitt, S. Krause, J.R. Cavey, D.E. Vinkemeier, U. Vinkemeier, A family-wide assessment of latent STAT transcription factor interactions reveals divergent dimer repertoires, J. Biol. Chem. 299 (5) (2023) 104703.
[20] X. Mao, Z. Ren, G.N. Parker, H. Sondermann, M.A. Pastorello, W. Wang, J. S. McMurray, B. Demeler, J.E. Darnell Jr., X. Chen, Structural bases of unphosphorylated STAT1 association and receptor binding, Mol. Cell 17 (6) (2005) 761–771.
[21] M. Zhong, M.A. Henriksen, K. Takeuchi, O. Schaefer, B. Liu, J. ten Hoeve, Z. Ren, X. Mao, X. Chen, K. Shuai, J.E. Darnell Jr., Implications of an antiparallel dimeric structure of nonphosphorylated STAT1 for the activation-inactivation cycle, Proc. Natl. Acad. Sci. U. S. A. 102 (11) (2005) 3966–3971.
[22] C. Mertens, M. Zhong, R. Krishnaraj, W. Zou, X. Chen, J.E. Darnell Jr., Dephosphorylation of phosphotyrosine on STAT1 dimers requires extensive spatial reorientation of the monomers facilitated by the N-terminal domain, Genes Dev. 20 (24) (2006) 3372–3381.
[23] U. Vinkemeier, S.L. Cohen, I. Moarefi, B.T. Chait, J. Kuriyan, J.E. Darnell Jr., DNA binding of *in vitro* activated Stat1α, Stat1β and truncated Stat1: interaction between NH_2-terminal domains stabilizes binding of two dimers to tandem DNA sites, EMBO J. 15 (20) (1996) 5616–5626.
[24] A. Begitt, M. Droescher, T. Meyer, C.D. Schmid, M. Baker, F. Antunes, K. P. Knobeloch, M.R. Owen, R. Naumann, T. Decker, U. Vinkemeier, STAT1-

cooperative DNA binding distinguishes type 1 from type 2 interferon signaling, Nat. Immunol. 15 (2) (2014) 168–176.
[25] X. Chen, U. Vinkemeier, Y. Zhao, D. Jeruzalmi, J.E. Darnell Jr., J. Kuriyan, Crystal structure of a tyrosine phosphorylated STAT-1 dimer bound to DNA, Cell 93 (5) (1998) 827–839.
[26] N. Wenta, H. Strauss, S. Meyer, U. Vinkemeier, Tyrosine phosphorylation regulates the partitioning of STAT1 between different dimer conformations, Proc. Natl. Acad. Sci. U. S. A. 105 (27) (2008) 9238–9243.
[27] Z. Zi, K.H. Cho, M.H. Sung, X. Xia, J. Zheng, Z. Sun, In silico identification of the key components and steps in IFN-γ-induced JAK-STAT signalling pathway, FEBS Lett. 579 (5) (2005) 1101–1108.
[28] K. Rateitschak, A. Karger, B. Fitzner, F. Lange, O. Wolkenhauer, R. Jaster, Mathematical modelling of interferon-γ signalling in pancreatic stellate cells reflects and predicts the dynamics of STAT1 pathway activity, Cell. Signal. 22 (1) (2010) 97–105.
[29] M. Droescher, A. Begitt, A. Marg, M. Zacharias, U. Vinkemeier, Cytokine-induced paracrystals prolong the activity of signal transducers and activators of transcription (STAT) and provide a model for the regulation of protein solubility by small ubiquitin-like modifier (SUMO), J. Biol. Chem. 286 (21) (2011) 18731–18746.
[30] H. Metwally, M.M. Elbrashy, T. Ozawa, K. Okuyama, J.T. White, J. Tulyeu, J. N. Søndergaard, J.B. Wing, A. Muratsu, H. Matsumoto, M. Ikawa, H. Kishi, I. Taniuchi, T. Kishimoto, Threonine phosphorylation of STAT1 restricts interferon signaling and promotes innate inflammatory responses, Proc. Natl. Acad. Sci. U. S. A. 121 (17) (2024) e2402226121.
[31] H. Metwally, M.M. Elbrashy, H. Kayama, K. Okuyama, I. Taniuchi, K. Takeda, T. Kishimoto, Threonine phosphorylation of STAT1 safeguards gut epithelial integrity and restricts interferon-mediated cytotoxicity, Proc. Natl. Acad. Sci. U. S. A. 122 (30) (2025) e2511957122.
[32] A. Begitt, T. Meyer, M. van Rossum, U. Vinkemeier, Nucleocytoplasmic translocation of Stat1 is regulated by a leucine-rich export signal in the coiled-coil domain, Proc. Natl. Acad. Sci. U. S. A. 97 (19) (2000) 10418–10423.
[33] A. Marg, T. Meyer, M. Vigneron, U. Vinkemeier, Microinjected antibodies interfere with protein nucleocytoplasmic shuttling by distinct molecular mechanisms, Cytometry A 73A (12) (2008) 1128–1140.
[34] D.T. Gillespie, Exact stochastic simulation of coupled chemical reactions, J. Phys. Chem. 81 (25) (1977) 2340–2361.
[35] N. Kudo, B. Wolff, T. Sekimoto, E.P. Schreiner, Y. Yoneda, M. Yanagida, S. Horinouchi, M. Yoshida, Leptomycin B inhibition of signal-mediated nuclear export by direct binding to CRM1, Exp. Cell Res. 242 (2) (1998) 540–547.
[36] T. Decker, P. Kovarik, Serine phosphorylation of STATs, Oncogene 19 (21) (2000) 2628–2637.
[37] I. Lödige, A. Marg, B. Wiesner, B. Malecová, T. Oelgeschläger, U. Vinkemeier, Nuclear export determines the cytokine sensitivity of STAT transcription factors, J. Biol. Chem. 280 (52) (2005) 43087–43099.
[38] B.L. Timney, B. Raveh, R. Mironska, J.M. Trivedi, S.J. Kim, D. Russel, S.R. Wente, A. Sali, M.P. Rout, Simple rules for passive diffusion through the nuclear pore complex, J. Cell Biol. 215 (1) (2016) 57–76.
[39] R.P. Andrews, M.B. Ericksen, C.M. Cunningham, M.O. Daines, G.K. Hershey, Analysis of the life cycle of STAT6, continuous cycling of STAT6 is required for IL-4 signaling, J. Biol. Chem. 277 (39) (2002) 36563–36569.
[40] I. Swameye, T.G. Müller, J. Timmer, O. Sandra, U. Klingmüller, Identification of nucleocytoplasmic cycling as a remote sensor in cellular signaling by databased modeling, Proc. Natl. Acad. Sci. U. S. A. 100 (3) (2003) 1028–1033.
[41] L. Liu, S. Okada, X.F. Kong, A.Y. Kreins, S. Cypowyj, A. Abhyankar, J. Toubiana, Y. Itan, M. Audry, P. Nitschke, C. Masson, B. Toth, J. Flatot, M. Migaud, M. Chrabieh, T. Kochetkov, A. Bolze, A. Borghesi, A. Toulon, J. Hiller, S. Eyerich, K. Eyerich, V. Gulácsy, L. Chernyshova, V. Chernyshov, A. Bondarenko, R. M. Grimaldo, L. Blancas-Galicia, I.M. Beas, J. Roesler, K. Magdorf, D. Engelhard, C. Thumerelle, P.R. Burgel, M. Hoernes, B. Drexel, R. Seger, T. Kusuma, A. F. Jansson, J. Sawalle-Belohradsky, B. Belohradsky, E. Jouanguy, J. Bustamante, M. Bué, N. Karin, G. Wildbaum, C. Bodemer, O. Lortholary, A. Fischer, S. Blanche, S. Al-Muhsen, J. Reichenbach, M. Kobayashi, F.E. Rosales, C.T. Lozano, S.S. Kilic, M. Oleastro, A. Etzioni, C. Traidl-Hoffmann, E.D. Renner, L. Abel, C. Picard, L. Maródi, S. Boisson-Dupuis, A. Puel, J.L. Casanova, Gain-of-function human STAT1 mutations impair IL-17 immunity and underlie chronic mucocutaneous candidiasis, J. Exp. Med. 208 (8) (2011) 1635–1648.
[42] F.L. van de Veerdonk, T.S. Plantinga, A. Hoischen, S.P. Smeekens, L.A. Joosten, C. Gilissen, P. Arts, D.C. Rosentul, A.J. Carmichael, C.A. Smits-van der Graaf, B. J. Kullberg, J.W. van der Meer, D. Lilic, J.A. Veltman, M.G. Netea, STAT1 mutations in autosomal dominant chronic mucocutaneous candidiasis, N. Engl. J. Med. 365 (1) (2011) 54–61.
[43] J. Petersen, J. Staab, O. Bader, T. Buhl, A. Ivetic, T. Meyer, Identification of a distinct subset of disease-associated gain-of-function missense mutations in the STAT1 coiled-coil domain as system mutants, Mol. Immunol. 114 (2019) 30–40.
[44] N. Ott, L. Faletti, M. Heeg, V. Andreani, B. Grimbacher, JAKs and STATs from a clinical perspective: loss-of-function mutations, gain-of-function mutations, and their multidimensional consequences, J. Clin. Immunol. 43 (6) (2023) 1326–1359.
[45] A. Singh, A. Jayaraman, J. Hahn, Modeling regulatory mechanisms in IL-6 signal transduction in hepatocytes, Biotechnol. Bioeng. 95 (5) (2006) 850–862.
[46] E. Shudo, J. Yang, A. Yoshimura, Y. Iwasa, Robustness of the signal transduction system of the mammalian JAK/STAT pathway and dimerization steps, J. Theor. Biol. 246 (1) (2007) 1–9.
[47] T. Maiwald, A. Schneider, H. Busch, S. Sahle, N. Gretz, T.S. Weiss, U. Kummer, U. Klingmüller, Combining theoretical analysis and experimental data generation reveals IRF9 as a crucial factor for accelerating interferon α-induced early antiviral signalling, FEBS J. 277 (22) (2010) 4741–4754.
[48] A.C. Greenlund, M.O. Morales, B.L. Viviano, H. Yan, J. Krolewski, R.D. Schreiber, STAT recruitment by tyrosine-phosphorylated cytokine receptors: an ordered reversible affinity-driven process, Immunity 2 (6) (1995) 677–687.
[49] A. Kumar, M. Commane, T.W. Flickinger, C.M. Horvath, G.R. Stark, Defective TNF-α-induced apoptosis in STAT1-null cells due to low constitutive levels of caspases, Science 278 (5343) (1997) 1630–1632.
[50] M. Chatterjee-Kishore, K.L. Wright, J.P. Ting, G.R. Stark, How STAT1 mediates constitutive gene expression: a complex of unphosphorylated STAT1 and IRF1 supports transcription of the LMP2 gene, EMBO J. 19 (15) (2000) 4111–4122.
[51] F. Kok, M. Rosenblatt, M. Teusel, T. Nizharadze, V. Gonçalves Magalhães, C. Dächert, T. Maiwald, A. Vlasov, M. Wäsch, S. Tyufekchieva, K. Hoffmann, G. Damm, D. Seehofer, T. Boettler, M. Binder, J. Timmer, M. Schilling, U. Klingmüller, Disentangling molecular mechanisms regulating sensitization of interferon α signal transduction, Mol. Syst. Biol. 16 (7) (2020) e8955.
[52] A.C. Pfeifer, J. Timmer, U. Klingmüller, Systems biology of JAK/STAT signalling, Essays Biochem. 45 (2008) 109–120.
[53] T. Meyer, A. Begitt, U. Vinkemeier, Green fluorescent protein-tagging reduces the nucleocytoplasmic shuttling specifically of unphosphorylated STAT1, FEBS J. 274 (3) (2007) 815–826.